J. Fluid Mech. (1993), *vol.* 252, *pp.* 499–523

Impingement of an unsteady two-phase jet on unheated and heated flat plates

By İ. BEDİİ ÖZDEMİR AND J. H. WHITELAW

Imperial College of Science, Technology and Medicine, Mechanical Engineering Department, Thermofluids Section, Exhibition Road, London SW7 2BX, UK

(Received 28 February 1992 and in revised form 19 January 1993)

This paper is concerned with an experimental investigation of the oblique impingement of an unsteady, axisymmetric two-phase jet on heated surfaces. Size and velocity were measured simultaneously with a phase-Doppler velocimeter, and the spatial distributions over the wall jet were found to be correlated with the interfacial activities as inferred from vertical velocity measurements in the vicinity of the wall. These results are discussed together with size measurements by a laser-diffraction technique to quantify the effect of the approach conditions of the inflowing jet droplet field and wall temperature in relation to mechanisms of secondary atomization.

Two mechanisms of secondary atomization were identified; the first did not involve direct wall contact and was due to the strain acting on the droplets by the continuous phase within the impingement region and was enhanced by thermal effects from the wall to cause breakup. The approaching velocity of the inflowing droplets to the plate was important to this process so that higher velocities increased the rate of strain within the impingement region and, consequently, the wall temperature promoting the secondary atomization shifted towards lower values. The second mechanism required direct wall contact and involved atomization of the film deposited on the wall by the impingement of the inflowing two-phase jet. With the penetration of high-speed inflowing droplets into the film, liquid mass was raised into the two-phase medium due to splashes from the film so that a new size class with larger droplets was generated. The resulting large droplets tended to stay close to the wall within the impingement region with small vertical velocities.

In between the injections, the suspended droplet field above the film oscillated normal to the plate as a cloud so that the impact of large droplets on the film resulted in coalescence with the film and the ejection of smaller numbers of small droplets. The unsteady wall jet flow, caused by the arrival of the spray at the plate, swept the vertically oscillating droplet cloud radially outwards so that the resulting radial transport caused the dynamics of the unsteady film to be correlated with the size characteristics of the unsteady wall jet. Based on this phenomenological description, a radial droplet transport equation is derived.

The correlation suggests that the secondary atomization with direct wall contact is the dominant process for the generation of a new size class within the wall flow and initiates the mutual interaction between the unsteady film and wall jet droplet field.

1. Introduction

This paper describes an investigation of the impingement of an unsteady two-phase jet on a heated surface and the resulting unsteady film deposited on the wall, as in the cylinders of an internal-combustion engine. As will be shown, the size characteristics

of the two-phase wall jet and the space–time structure of the unsteady film are coupled through interfacial activities of the droplet field across the upper surface of the film, which is a complex interface between the film and the dense two-phase flow above it. The main purpose is to quantify this correlation and to explore the nature and implications of the downwash action of radial wall jets. The basic features of the spray–wall interaction are discussed in the following paragraphs.

The literature on the impaction processes of individual droplets is extensive but comprehensive understanding remains elusive, and spray impingement with many droplets and droplet–surface interaction is even more difficult to analyse. Aspects of the droplet–wall interaction have been investigated with impingement of isolated droplets onto hot surfaces, for example by Wachters & Westerling (1966) and Cumo & Farello (1967) and, as a consequence, heat transfer and evaporation have been evaluated as functions of surface temperature, droplet size and the normal and tangential components of the droplet velocity. The state of the environment surrounding the droplet is also a factor so that the evaporation and heat transfer rates can be larger in dry air than in a saturated atmosphere (Wachters, Bonne & Van Nouhuis 1966*a*). Zhang & Gogos (1991) have examined the vapour layer between the droplet and the surface, referred to as a spheroidal state and the corresponding surface temperature as the Leidenfrost temperature, and shown that it can affect heat transfer and evaporation dramatically. The spheroidal state can be maintained at surface temperatures below the boiling point of the liquid as long as the droplet and the surface temperatures are above the wet bulb temperature associated with the surrounding atmosphere. In the case of spray impingement with droplet interactions, the spheroidal state can occur at much higher surface temperatures than the boiling point with considerable wall wetting in the range from boiling point to the Leidenfrost temperature, above which the evaporation rate decreases owing to the low conductance of the vapour layer trapped under the droplets (Wachters *et al.* 1966*b*). A definite transition from wetting to non-wetting impact for individual droplets was also observed by Pedersen (1970) so that high heat transfer occurred in the wetting state with nucleate boiling as the droplets spread out in a thin film over the surface, while heat transfer characteristics had similar velocity dependence for all the sizes in the non-wetting state. Hoogendoorn & Hond (1974) showed that clusters of droplets with different sizes and velocities led to a Leidenfrost temperature different from that of a single droplet and that it increased with spray density. In the case of a spray, therefore, the influence of the size of individual droplets on the impaction and heat transfer processes is replaced by that of the size distribution of the droplet field. In addition, Gallily & La Mer (1958) reported that a fraction of droplets bounced from the surface on first contact and this behaviour changed with the velocity and size of the particles, as confirmed by Ranz & Hofelt (1957).

An important aspect of the interaction between a dense spray and a wall is that droplets may strike a solid wall and form a liquid film only if they expel and rupture the intervening air–vapour film (Dimitrov & Ivanov 1978; Pandit & Davidson 1990). Thus, the air–vapour gas field surrounding the droplets and the flow field of the continuous phase play an important role in binary interactions (Ashgriz & Poo 1990) by controlling the rupture of the intervening film. Jayaratne & Mason (1964) investigated the conditions for coalescence and rebound of isolated water droplets at an air–water interface and showed that, for a droplet of given size and velocity, there are sharply defined alternating ranges of impacting angles in which coalescence and bouncing occur. Large droplets coalesced with the plane surface at large impact angles with respect to the surface normal and this process decreased rapidly as the impact

velocity was reduced. A droplet of a given size failed to coalesce whatever the angle of impact if the impact velocity exceeded a critical value. Droplets impacting at nearly grazing incidence had little penetrating power and tended to skim the surface or bounce unless the impact velocity was very low. However, a large velocity tangential to the surface has been known (Yao & Cai 1985) to destabilize the droplets by increasing the deformation during impact.

A few investigations have been devoted to the phenomenon of spray impingement in internal combustion engines and most are related to the structure of the emerging jet and the temporal and spatial evolution of the spray in in-cylinder flows (Reitz & Bracco 1979, 1982; Fujimato *et al.* 1983; Bracco 1985). Hori & Sugiyama (1980) made an in-situ investigation of the gas movement process using Schlieren and ciné photography in conjunction with gas sampling and showed that the influence of air swirl on the spray was stronger after wall impingement and that swirl accelerated the formation of a homogeneous mixture. Katsura *et al.* (1989) investigated the impingement of a single spray on the piston cavity wall in a high pressure environment by photographing the temporal evolution of the spray and using a light extinction method to determine the spatial concentration distribution. Naber & Reitz (1988) simulated numerically the impingement of the spray on the piston head including the effects of breakup, collision and coalescence of droplets and gas turbulence, and showed that small droplets approaching the wall were deflected by the flow field of the large droplets impinging on the wall. Comparison of their results with experiments showed that the computed spray had a divergence angle of 10° in contrast to the measured value of 20°.

The aim of the investigation described in this paper was to study the consequences of the pulsatory impingement of a droplet cluster onto the film deposited on a heated plate and the subsequent mechanisms of droplet generation by the material torn or ejected from the film. As the spray in internal combustion engines is at much higher ambient density and temperature than that in atmospheric conditions, some differences in drop size, evaporation rate and breakup length may exist and, therefore, the present two-phase jet represents an early stage in examining the engine spray situation. The next section describes the experimental techniques, and the third presents and discusses the results. The paper ends with conclusions and an appraisal of the transport properties of the wall jet.

2. Flow configuration, instrumentation, and experimental procedures

2.1. *Experimental arrangement*

The experimental arrangement of figure 1 comprised an injection system (Bosch) consisting of four multi-hole nozzles connected separately to a distributor-type pump by high-pressure tubes of 305 mm length and 1.6 mm inner diameter. The fuel pump was driven by a d.c. motor of 1.5 kW power resulting in a repeated injection sequence at different frequencies as required by the experiment. The speed was monitored by a shaft encoder and stabilized by a closed-loop d.c. motor controller at 1000 ± 1 r.p.m. or better. The nozzles consisted of five holes of exit diameter $d_E = 210$ μm and 1 mm length oriented at different angles to the nozzle axis. Three nozzles injected into a dummy chamber and one jet of the fourth nozzle was allowed to impinge onto the heated plate while the sprays emerging from the other holes were sucked by a tip-mounted collecting piece and then diverted into a tank. The flow rate was adjusted by means of the pump speed and the mechanical governor which set the length of the stroke. The tension of the needle spring determined the speed and duration of the

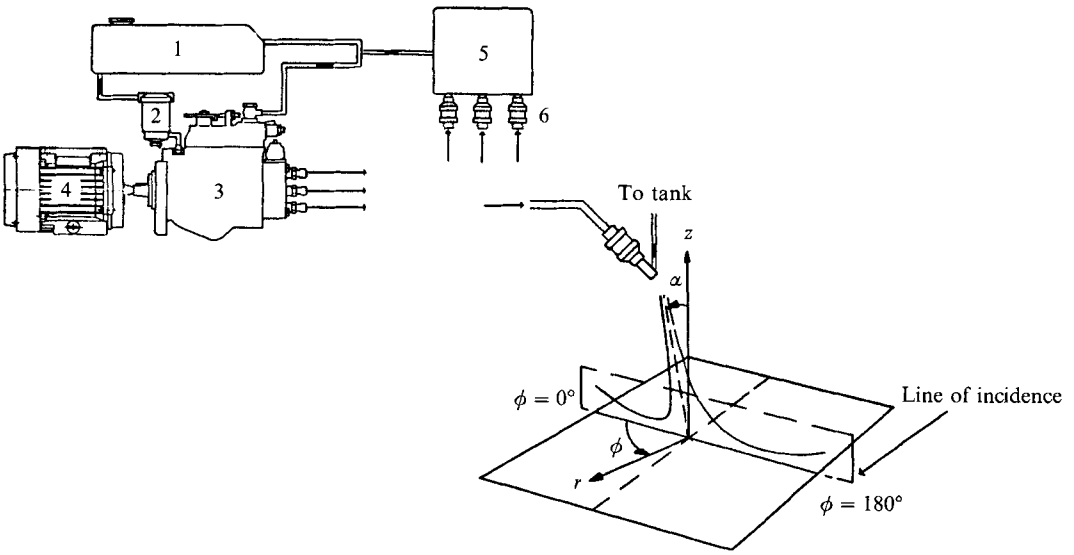

FIGURE 1. General arrangement of the experimental set-up: 1, Fuel tank. 2, Filter. 3, Pump. 4, d.c. motor. 5, Dummy chamber. 6, Injectors.

opening of the nozzle needle, and an opening pressure of 20 bars provided flow rates with nozzle exit velocities within the range of the maximum Doppler frequency of the PDV signal processor, details of which are given in §2.2. Traces of the inverted obscuration signal produced by a photodiode placed against the laser beam crossing the spray axis at the nozzle exit are shown in figure 2 (upper trace) together with the signals from the Hall-effect needle lift sensor (ASM Type TSM-250). Results were obtained for frequencies in the range 8.4–16.7 Hz and, except for the injection at 16.7 Hz with a volume flow rate of 7.2 mm^3/injection per hole, in which the bulk of the volume was released within the first 2 ms with a total injection period of 4.6 ms, all results exhibited an injection history with two obscuration-peaks, as in figure 2(*b*), indicating two major pulses of fluid. The diffraction-based size measurements were made at two extreme conditions; a low injection rate of 8.4 Hz with a volume flow rate of 1.2 mm^3 per injection, and a high injection rate of 16.7 Hz with a volume flow rate of 7.2 mm^3. Detailed documentation of the wall jet droplet field corresponded to 16.7 Hz injection frequency with a volume flow rate of 7.2 mm^3, and this operating condition was the same as that of Özdemir & Whitelaw (1992*a*) in measuring the unsteady component of the thickness of the film deposited on the wall.

The spray impinged with a nozzle-to-plate distance of $H = 30$ mm ($H/d_E = 143$) and at an angle of incidence, α, of 20° onto the hot plate (Rowenta Model WP), controlled at constant surface temperatures of 23, 50, 100, 150 and 240 °C by means of a voltage regulator. The plate was placed horizontally so as to minimize the effect of the gravity on the wall-jet and the film deposited on the wall. Before the start of the injection process, the uniformity of the surface temperature distribution over the plate was checked with surface-mounted copper–constantan thermocouples and was found to be within ± 0.5 °C over an area of 200 cm^2. The deviation of surface temperature during the process of injection from that without injection was negligible owing to the large thermal inertial of the heated plate.

The fluid was multi-component diesel fuel (Shell Gas Oil SH) with a density of 844.3 kg/m^3 (at 15 °C) and a relative refractive index, n', of 1.43. The distillation data and some other properties of the fluid are given in table 1.

(*a*)

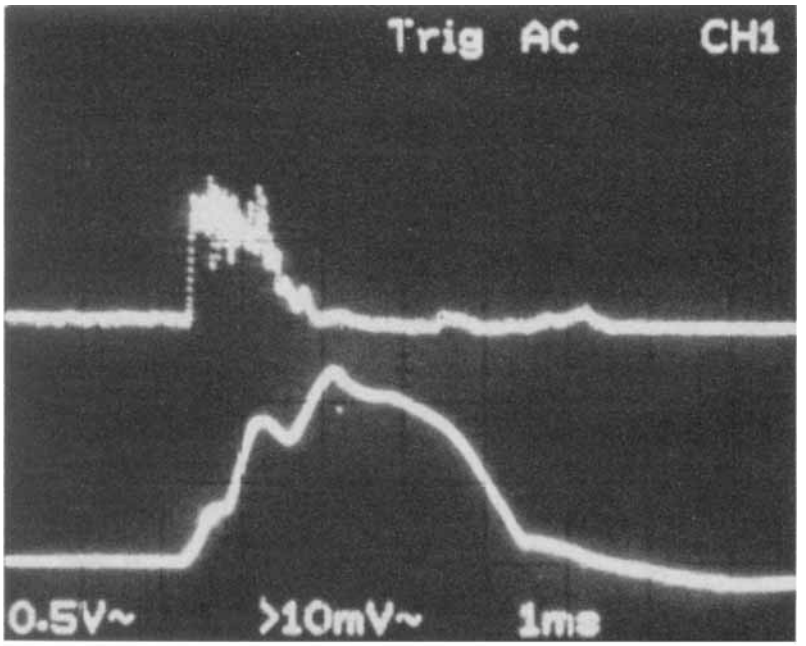

(*b*)

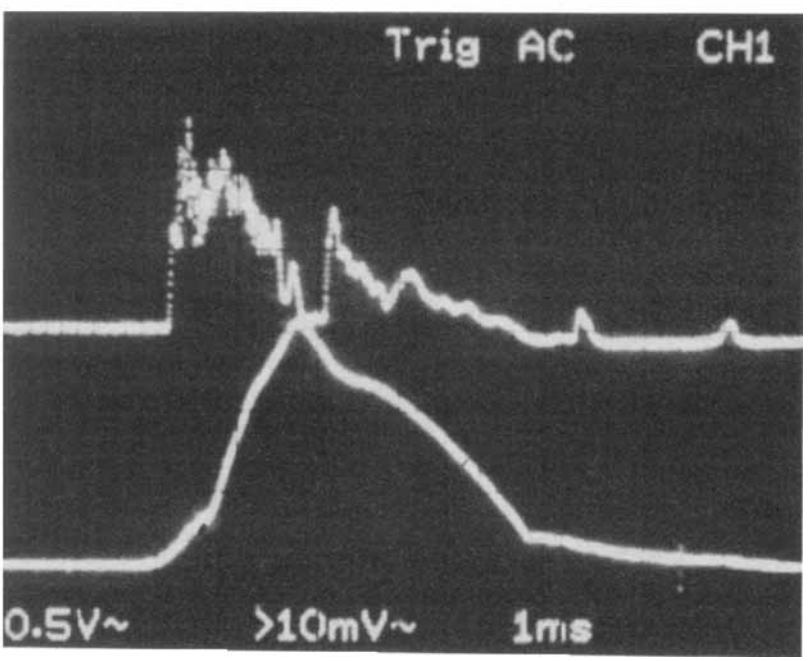

FIGURE 2. Injection histories for (*a*) f_{inj} = 16.7 Hz with volume flow rate of 7.2 mm^3/inj; (*b*) f_{inj} = 8.4 Hz with volume flow rate of 1.2 mm^3/inj.

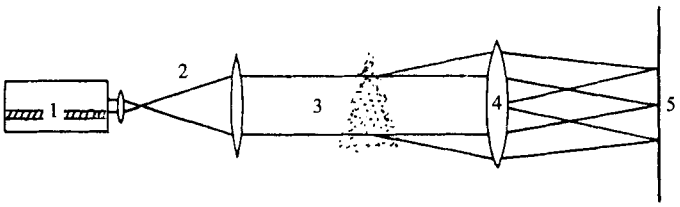

FIGURE 3. Schematic of the laser-diffraction system: 1, Laser. 2, Transmitting optics. 3, 9-mm diameter beam. 4, Fourier transform lens. 5, Diode plane.

Kinematic viscosity	3.5×10^{-6} m²/s (at 40 °C)
Surface tension	27 mN/m
Gross calorific value	46 140 kJ/kg
Cetane index	56.5

Distillation data

	(°C)
IBP	175.0
10 % Rec.	224.5
20 %	250.0
30 %	267.5
40 %	278.0
50 %	287.5
60 %	296.5
70 %	306.5
80 %	319.0
90 %	335.0
FBP	369.0
Recovery (% volume)	99.0

TABLE 1. Properties of the fluid

2.2. *Size measurements based on diffraction and phase; description of the systems, limitations and accuracy*

A diffraction-based size measurement technique was used to investigate the effect of approach conditions of the inflowing droplet field and of the wall temperature on the size characteristics of the impinging two-phase jet. The system (Malvern 2600C) is shown in figure 3 and comprised a 5 mW He–Ne laser and a transmitting optics, which produced a collimated 9 mm diameter beam (at the e^{-2} intensity points), and light scattered in the near forward direction was focused by a receiver lens of 300 mm focal length onto a set of thirty-one annular concentric ring diodes, converting the angular scattering pattern into a radial distribution at the diode plane, from which a 15-parameter size distribution was obtained iteratively. This, so-called model-independent approach, was appropriate to avoid smoothing of experimental data in the regions where the size distribution was bimodal. In order to associate the data collected to a specific phase of the injection cycle, the measurements were gated externally to a TTL (transistor–transistor logic pulse) of 2.5–5.0 V signal which caused a data packet to be transferred to the computer for a period of 10 μs centred at $t = 2.5$ ms. Even though the diffraction-based size measurements are straightforward, there are limitations which require careful design of the experiments. When the sample concentration was high, light diffracted from one droplet could be scattered by other droplets in the

measurement volume before reaching the receiving optics, resulting in a diffraction pattern with larger scattering angle (Dodge 1984). Felton, Hamidi & Aigal (1985) suggested that multiple scattering effects increased gradually and were insignificant for obscuration less than 0.5, above which corrections were recommended since the light energy distribution was shifted towards larger diode numbers and resulted in size distributions which were broadened and shifted towards smaller droplet sizes. However, the corrections suggested by Dodge (1984) and Felton *et al.* (1985) were for Rosin–Rammler and Log–Normal distributions and cannot be applied to the model-independent distributions and, therefore, no correction was implemented to the data presented in §3.1. Besides, the correction based on a single value of obscuration may be unreliable (Cossali & Hardalupas 1992), because obscuration can vary over the 9 mm-interrogation beam. This stems from the fact that the spray with narrow cone angle could occupy only a small portion of the beam while the rest of the beam fell directly onto the central diode resulting in non-uniform obscuration with larger actual values in the spray than those measured by the cental diode. In the present case, the obscuration measured by the central diode was less than 0.5 for wall temperatures below 240 °C, above which it exceeded this limit owing to the increase in number density with secondary atomization and this is discussed in detail in §3.1. It is known (Hirleman, Oechsle & Chigier 1984) that an increase in the sample-to-lens distance beyond the focal length of the receiving lens results in uncertainties owing to the vignetting or truncation of the small droplets scattering signal and, thus, a 300 mm focal-length lens (with the corresponding size range of 5.8–564 μm) was preferred since it included the entire volume of the sample within the selected focal length. In order to ensure that conditions did not change during data collection and to avoid droplet deposition on the collimating and collecting lenses, high-quality glass plates were placed in front of the lenses and were cleaned for every 200 acquisition sweeps of the light energy distribution. Each measurement, thus, consisted of five sets of 200 sweeps of the spray (so that the alignment procedure had to be repeated after each set) and the results were averaged. The results presented in §3.1 are the volume size distributions of all the droplets contained in the cylindrical measurement volume over a range of size bands and no further spatial resolution was possible by deconvoluting the results as in the case of an axisymmetric field (Hammond 1981). The intensity distribution of the 9-mm laser beam was Gaussian so that the contribution of small droplet sizes could be underestimated since they experience a smaller measurement volume than large droplets, but this was unimportant compared to the uncertainties caused by the obscuration and no further measures were taken. Beam steering or wander due to thermal or density gradients in the beam path was negligible so that it did not cause the observation of undiffracted light by the innermost diode, as described by Meyer & Chigier (1986).

The PDV system of figure 4 was used to measure the velocity and size characteristics of the two-phase impinging jet, and comprised a 35 mW He–Ne laser (Spectra Physics Model 107B), a purpose-built transmitting optics, a receiving optics (Aerometrics Model RCV-2100), a signal processor (Aerometrics PDP-3100), and a microcomputer (Dell 386). In order to associate the data with a specific phase of injection cycle, PDV measurements were gated to an external TTL signal, conditioned by an oscilloscope (Philips PM3217) and activated by a signal from the needle lift-sensor. An ensemble of (at least) 5000 data items was collected within a 100 μs time interval which was centred at $t = 2$ and 3.5 ms with respect to the needle lift when the velocity–size characteristics of the two-phase wall flow were measured and at various times when inlet conditions of the inflowing spray were documented. Because the particle density in the spray was

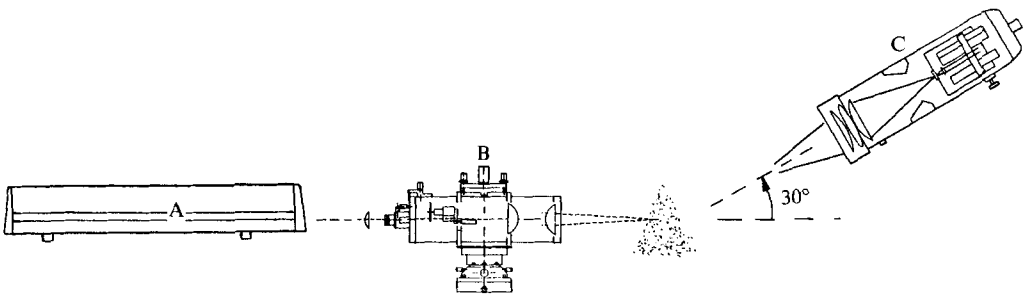

FIGURE 4. Schematic of the phase-Doppler system. A, Laser. B, Transmitting optics. C, Receiving optics.

	Laser
Beam diameter	1.250 mm (at e^{-2} intensity locations)
Wavelength	0.6328 μm
	Transmitting optics
Grating lens	100 mm
Collimating lens	300 mm
Imaging lens	400 mm
Grating line pairs	4096/8192*/16384
Beam separations	17.7/33.0*/62.6 mm
Frequency shift	3.48 MHz
(* indicates the values that were used in this study)	
	Control volume
Fringe spacing	7.647 μm
Beam waist	257.826 μm
	Receiving optics
Collection angle	30°
Lens system	f/5 achromatic doublet, 495 mm, and f/2.2 triplet, 220 mm
Receiver aperture	50 μm slit
	Fluid properties
Refractive index	1.43

TABLE 2. PDV optical parameters

relatively high (of the order of $\sim 4 \times 10^3/\text{cm}^3$), the presence of more than one particle in the control volume resulted in noisy signals, and increased the rate of data rejection owing to the validation criteria which required the ratio of two independent phase measurements between the pairs of three photodetectors to fall within a preset tolerance of 1%. These uncertainties were minimized by truncating the size of the control volume with a 50 μm slit and by reducing the photomultiplier voltage which required care since it could also bias the distributions towards larger droplets, as small droplets would not be detected unless they passed near to the centre of the Gaussian beam. Another approach to decrease the size of the control volume was to use larger beam separation, but this was not pursued because it contradicted the requirement of a large conversion factor (fringe spacing, see also table 2) to cope with the large velocities involved, since the signal processor was limited to a maximum Doppler signal frequency of 16 MHz. Also, because the PDV control volume was configured to measure the radial velocities of the wall flow with fringe planes perpendicular to the

plate, some of the droplet trajectories were highly oblique to the control volume within the impingement region where the flow direction was not known *a priori*. Frequency shift (3.48 MHz) ensured that all droplet trajectories (and so the size classes) produced sufficient Doppler cycles in the burst (in the present investigation, eight cycles were required to validate the measurements) so that they had similar probabilities of detection.

2.3. *Presentation of the size measurements*

In order to facilitate comparison of experimental data, it is common practice to reduce the size distribution information to a single mean droplet diameter which, while facilitating the comparisons, also discards information. When the process controlling droplet size depends on the droplet volume and surface area (Lefebvre 1989), such as heat or mass transfer, the Sauter mean diameter, d_{32}, is appropriate to describe the drop diameter having the same volume to surface ratio as the whole spray sample, which also avoids the problem that very small or very large droplets can dominate the single mean value (Meyer & Chigier 1986). For an infinite size range of droplets, d_{32} is defined as

$$d_{32} = \frac{\int_0^\infty s(d)\, d^3\, \mathrm{d}d}{\int_0^\infty s(d)\, d^2\, \mathrm{d}d}. \tag{1}$$

For a finite range, such as the fifteen size classes used in the laser diffraction technique, this yields

$$d_{32} = \frac{\sum_{i=1}^{15} s_i d_i^3}{\sum_{i=1}^{15} s_i d_i^2} = \frac{\sum_{i=1}^{15} \mathscr{S}_i}{\sum_{i=1}^{15} \mathscr{S}_i / d_i}, \tag{2}$$

where s_i and $\mathscr{S}_i$ are the number and the total volume of the droplets having diameter d_i.

3. Results and discussion

3.1. *Characteristics of the droplet field*

The diffraction-based size measurements were averaged along the line-of-sight of the interrogation beam and the results were, therefore, limited to the interrogation beam centred at $z = 5.5$ mm above the plate and crossing the droplet field perpendicular to the line of incidence at three radial positions, $r = 7$ mm along the $\phi = 0°$ direction, the geometrical impingement point, $r = 0$, and $r = 7$ mm along the $\phi = 180°$ direction. This provided information of the effect of plate temperature and jet exit conditions on the size characteristics of the droplet field and, based on this information, the operating conditions for the detailed local measurements of wall flow field using PDV were chosen. The results of figure 5 represent size characteristics of the two-phase wall jet at the injection stage, $t = 2.5$ ms, after needle lift for five plate temperatures including $T_w = 23$, 50, 100, 150, and 240 °C and two jet exit conditions. For low injection frequency and flow rate, the obscuration (see figure 5*a*) remained insignificant over a large range of plate temperatures with values of 0.5 and greater confined to wall temperatures of 175 °C and above and, as a result, the uncertainties in size measurements were low so that a consistent decrease of droplet size with wall

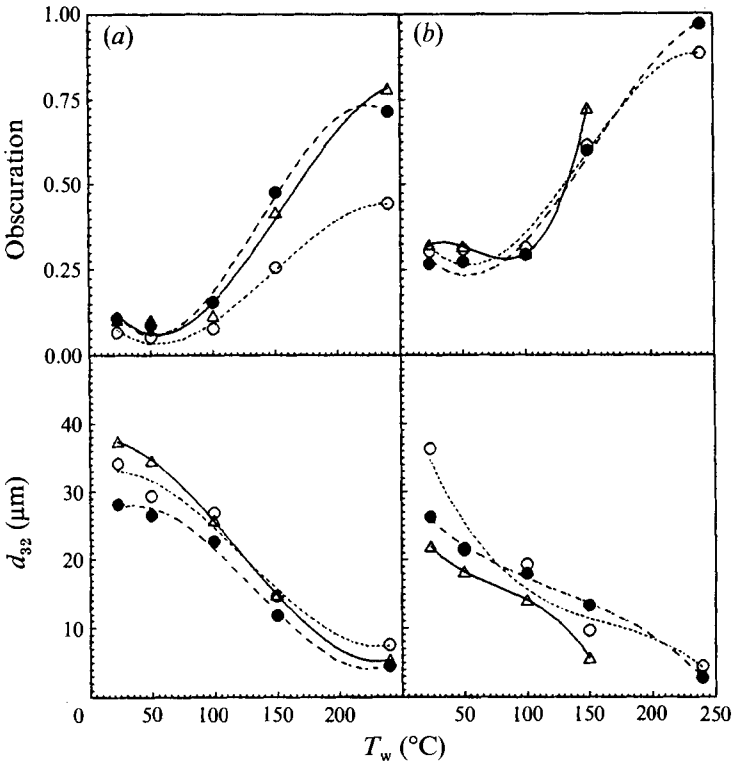

FIGURE 5. Variation of the droplet size with wall temperature for two nozzle exit conditions; $t = 2.5$ ms after needle lift. (*a*) $f_{inj} = 8.4$ Hz with volume flow rate of 1.2 mm³/inj; (*b*) $f_{inj} = 16.7$ Hz with volume flow rate of 7.2 mm³/inj. ○, $r = 7$ mm along the $\phi = 0°$ direction; ●, $r = 0$, geometrical impingement point; △, $r = 7$ mm along the $\phi = 180°$ direction.

temperature was observed for the three locations of the interrogation beam. The obscuration results suggest that, at higher wall temperatures, secondary atomization within the impingement region increased the number density of the droplet field for nearly the same amount of mass, which was previously within a small number of large droplets, so that the transparency of the resulting fog was much lower, i.e. the obscuration was higher owing to the multiple scattering effects as explained in §2.2. The increase in the obscuration above 175 °C is also associated with the initiation of the process of evaporation of low boiling point hydrocarbons of the multi-component fluid, as consistent with the distillation data presented in table 1. However, the decrease in the accuracy of the size measurements at the higher wall temperatures is unimportant, since the droplet sizes are below 8 μm. It is apparent that the droplet size, when the plate was unheated and at a temperature of 23 °C, was different for the three locations of the interrogation beam such that the average droplet size was smaller at the centre ($r = 0$) than at $\phi = 0°$ and 180°. Since the average size at $r = 0$ was dominated by the inflowing two-phase jet, which had not yet interacted with the plate, the results indicate that larger droplets are generated during the impingement on the unheated plate and this is more evident in the $\phi = 180°$ direction, which was the major flow direction of the inflowing droplets. This argument is consistent with the implications of the measurements of the unsteady component (temporal variations) of the film thickness reported by Özdemir & Whitelaw (1992*a*), that when the peak values (of the order of half a millimetre) of the unsteady component of the film thickness increases

with wall temperature, given the absolute values of the order of a millimetre, a thicker steady film forms if the plate is at lower temperatures and this increases the likelihood of splashes owing to the penetration of the inflowing droplets. The droplets ejected to wall jet are expected to have larger sizes and smaller velocities than the inflowing droplets. The difference in the droplet sizes at the three locations decreases at higher wall temperatures, indicating fewer splashes as the steady film thickness decreases with increased plate temperature. Also, it can be inferred from the average droplet size at the centre, which represents the inflowing jet, that information of the thermal characteristics of the plate was transported upstream to the inflowing jet before impingement so that the average size of the approaching droplet field of the inflowing jet decreased with the wall temperature.

The results so far show that secondary atomization occurs in two ways: either at the wall, owing to the direct contact of the inflowing droplets with the unsteady film, or by a mechanism through which the kinematics of the continuous phase play an important role and this process is promoted by thermal effects within the impingement region. In the latter case, the strain field of the continuous phase within the impingement region deforms the inflowing droplets so that the surface tension, which is reduced by heat transfer from the wall, can no longer sustain the large mass of the inflowing droplets intact and breakup occurs until the surface tension can balance the strain. It remains to quantify the extent to which breakup occurs in the radial wall jet owing to the strain and reduction of the surface tension, and owing to the splashes from material torn from the unsteady film. Leaving the detailed discussion of the breakup mechanism with splashes from the film to §3.3, it suffices here to say that the size characteristics of the wall jet should show less correlation with the unsteady film if the strain mechanism dominates.

For the higher injection frequency and flow rate, figure 5(*b*), where the nozzle exit velocities were higher than the low injection frequency and flow rate, the obscuration exceeded 0.5 in a wall temperature range extending down to 135 °C. This temperature is lower than 175 °C which was the lowest wall temperature at which obscuration exceeded 0.5 for the low injection frequency and flow rate. This is because, at higher nozzle exit velocities, the strain of the continuous phase acting on the droplets within the impingement region can be sufficiently large to overcome higher values of surface tension so that breakup leading to secondary atomization (indicated by an increase in number density) can take place even at lower surrounding temperatures. Although the scatter in d_{32} indicates the increased uncertainties, it is still evident that the differences in droplet sizes with position again diminish with wall temperature. Contrary to the previous operating condition, however, smaller droplets exist in the $\phi = 180°$ direction with the plate unheated.

With this knowledge of the effects of plate temperature and jet exit conditions, the more detailed investigation of the droplet field of the wall flow was carried out with the high injection frequency and flow rate (16.7 Hz and 7.2 mm^3/injection) with plate temperatures of 150 and 240 °C. This choice of nozzle exit condition was compatible with the thickness measurements of Özdemir & Whitelaw (1992*a*), where the inversion process required the film to attain a single maximum during the whole injection cycle. To relate the characteristics of the wall flow with those of the inflowing jet, the upstream conditions of the inflowing two-phase jet were measured but it was impossible to measure very close to the nozzle exit where the spray was very dense so that the conditions at 16 mm (76 d_E) downstream of the nozzle exit with the plate removed were taken as the initial conditions of the wall flow. At the beginning of the injection, figure 6(*a*), the d_{32} decreases from 80 μm to a minimum of 70 μm at

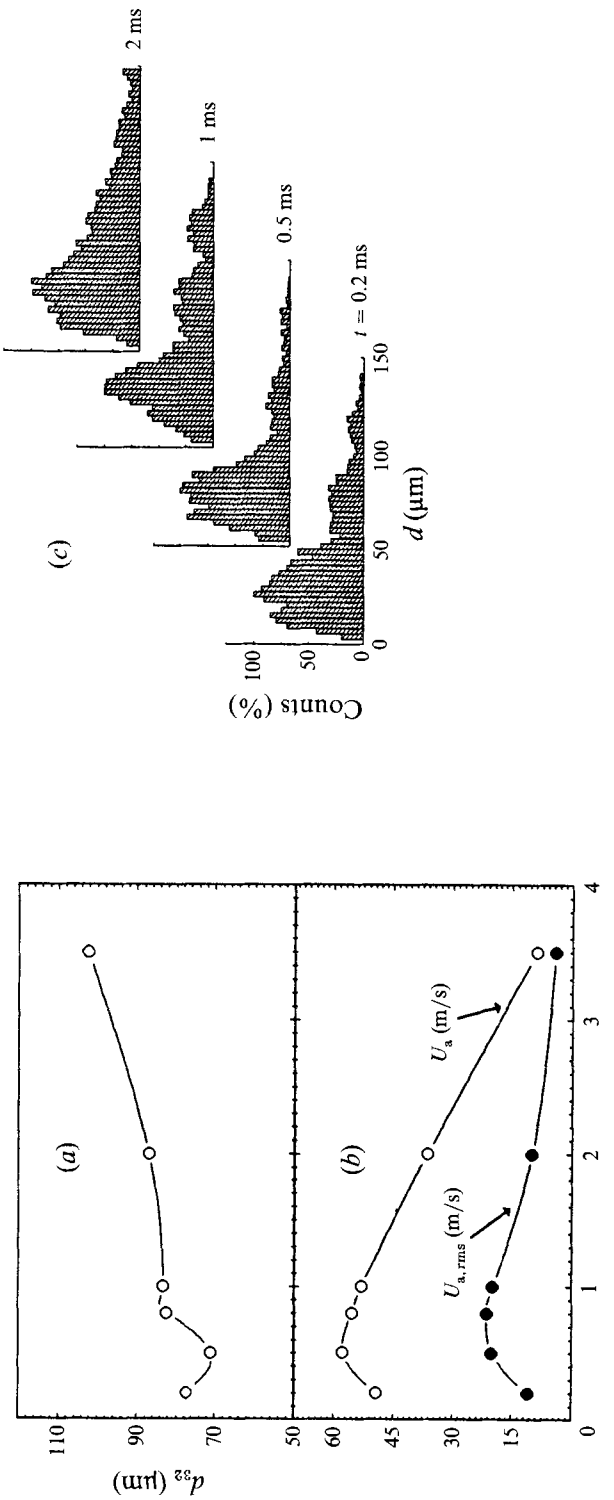

FIGURE 6. Temporal variations of the droplet field at the centreline of the jet and 16 mm downstream of the nozzle exit. (*a*) Sauter mean diameter. (*b*) Mean and r.m.s. values of the axial velocity. (*c*) Size distribution.

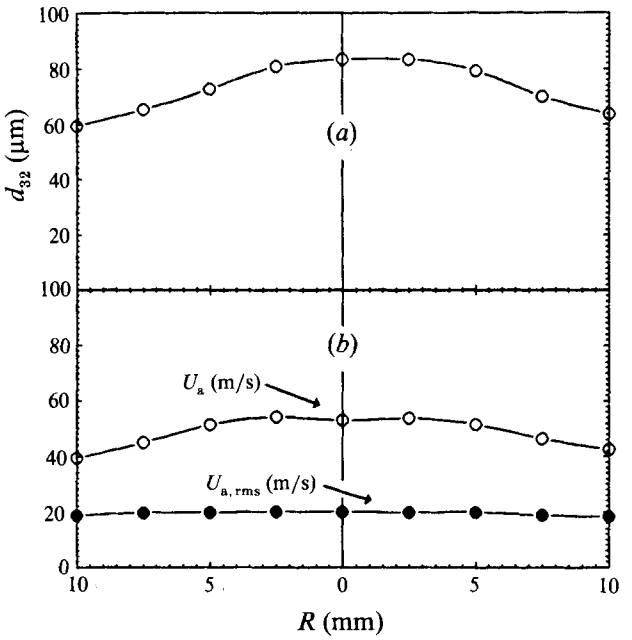

FIGURE 7. Radial profiles at 16 mm downstream of the nozzle exit and $t = 1$ ms after needle lift. (*a*) Sauter mean diameter. (*b*) Mean and r.m.s. values of the axial velocity.

$t = 0.5$ ms, followed by a rapid increase to 84 μm and then, with a gradual rise, it reaches 100 μm at $t = 3.5$ ms. The histograms of figure 6(*c*) show several peaks and, particularly at the later stage of the injection, $t = 2$ ms, the size distribution extends irregularly beyond the upper limit of the size range. This reveals imperfect atomization during the transient of needle closure with non-spherical droplets and possibly ligaments which were perceived by the PDV instrument as large spherical droplets and skewed the size distribution towards larger sizes which dominated d_{32}. An attempt to exclude these measurements by limiting the size range had an even more dangerous consequence in that valid measurements were rejected. Thus, setting the size range of the PDV required experience to ensure that the skewness introduced by non-spherical droplets was negligible. The maximum mean axial velocity of figure 6(*b*) is around 60 m/s and coincides with the time of the minimum droplet diameter, and the mean velocity decays gradually at later periods of the injection so that significant velocities exist even at $t = 3.5$ ms after needle lift. The r.m.s. of the axial velocity decreases gradually with time from a maximum of 20 m/s to a value of 4.5 m/s. The radial profiles of the d_{32} and the axial velocity at $t = 1$ ms after needle lift, figure 7, exhibit symmetry with a fairly uniform distribution of r.m.s. values at around 19 m/s.

Local characteristics of the wall flow droplet field were measured at fourteen radial positions along the line of incidence extending from $r = 17.5$ mm in the $\phi = 0°$ direction to $r = 33$ mm in the $\phi = 180°$ direction with surface temperatures of 150 and 240 °C, and at distances of $z = 1$, 2, 3 and 4 mm above the plate. Figure 8 shows the variation of droplet size along the line of incidence for $t = 2$ and 3.5 ms, and it is clear that there is a larger wall temperature effect at the earlier time where (figure 8*a*) there is a single peak around the impingement point for $T_w = 150$ °C which increases with distance from the wall and attains a value of 40 μm at $z = 4$ mm. This maximum is representative of the approaching spray without wall interaction, and is almost half the value measured at the spray axis 76 d_E downstream of the nozzle exit where the

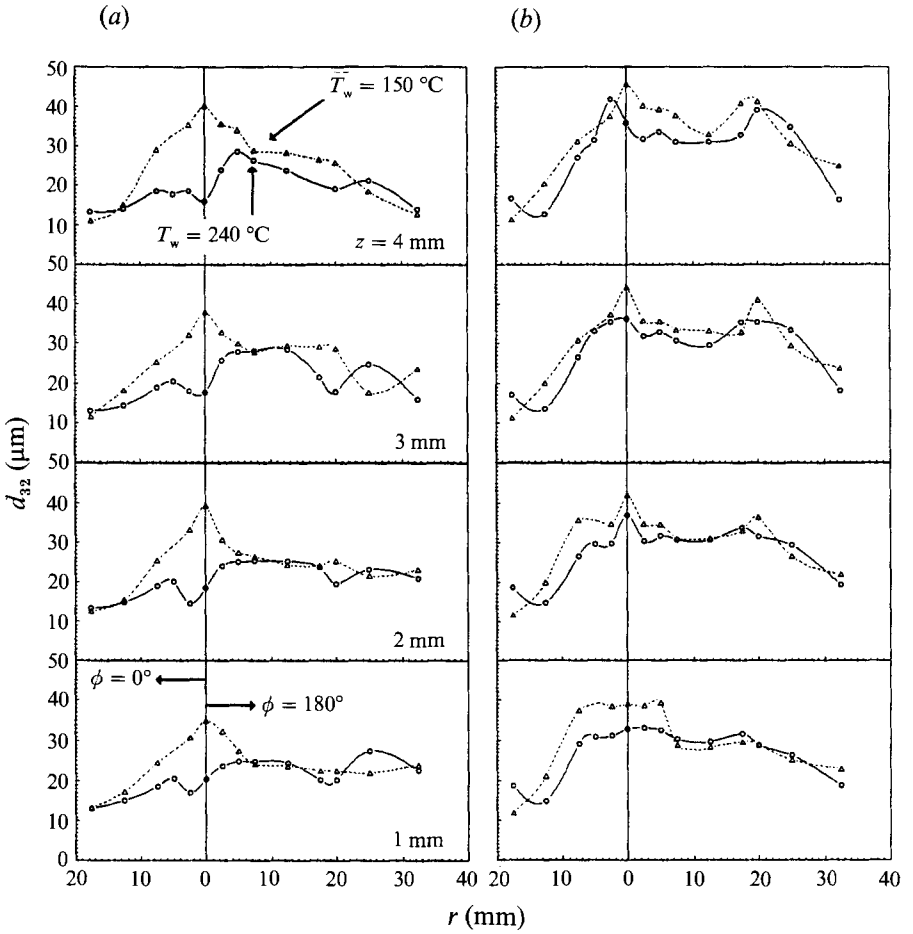

FIGURE 8. Variation of the droplet size along the line of incidence; f_{inj} = 16.7 Hz with volume flow rate of 7.2 mm³/inj. (*a*) t = 2 ms after needle lift; (*b*) t = 3.5 ms after needle lift.

minimum was 70 μm (figure 6*a*). When the wall temperature is increased to T_w = 240 °C, around the geometrical impingement point and particularly at z = 4 mm, the droplet size falls sharply with the stronger influence of the wall but without direct contact. The three peaks, two located in the ϕ = 180° direction and one in the ϕ = 0° direction, are well correlated with the distribution of the variation of the unsteady film reported by Özdemir & Whitelaw (1992*a*) along the line of incidence and this indicates the dominance of the secondary atomization with direct contact over the secondary atomization due to strain exerted by the continuous phase.

At the later stage of injection, t = 3.5 ms, maxima are located at the geometrical impingement point and at r = 20 mm in the ϕ = 180° direction, and are apparent away from the wall in figure 8(*b*). At large distances from the wall, the maximum diameter at r = 0 is around 40 μm for both wall temperatures which is nearly the same as the value at the same location when t = 2 ms but at the lower wall temperature of 150 °C. This can be explained by the small velocities involved at the later stages of injection so that the thermal effects were not sufficient to promote secondary atomization without contact.

Within the impingement region, the size histograms of figure 9(*a*), corresponding to figure 8(*b*) with t = 3.5 ms, are bimodal very close to the wall and turn gradually into

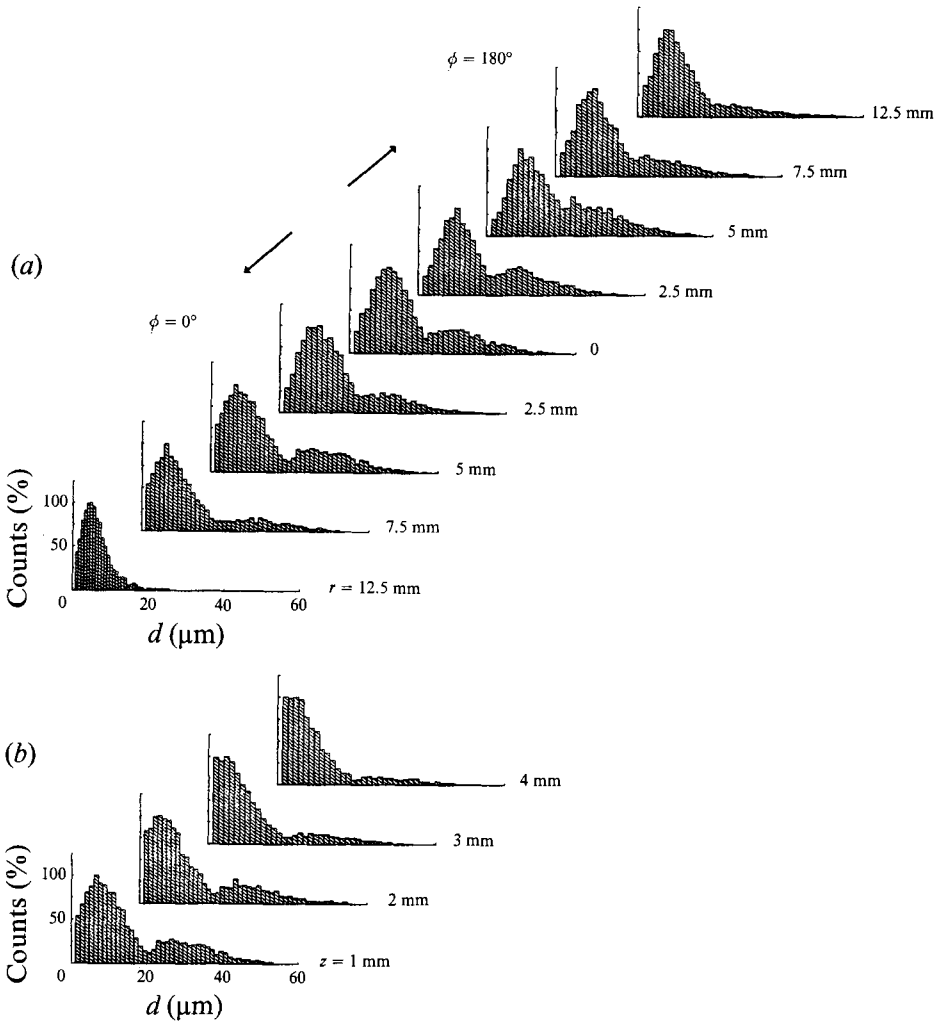

FIGURE 9. Change in the characteristics of the size distribution, T_w = 240 °C, and t = 3.5 ms (*a*) with radial position along the line of incidence at z = 1 mm; (*b*) with wall distance at r = 5 mm along the ϕ = 0° direction.

unimodal distributions for large radial distances, $r \geqslant 12.5$ mm. This was also true for T_w = 150 °C. In contrast to figure 6(*c*), the bimodal distributions diminish properly at the upper limit of the size range so that the second peak is not contaminated with the uncertainty due to the presence of non-spherical droplets. Indeed, it can be argued that the second peak represents a new size class of larger diameter droplets generated during the penetration of inflowing droplets into the unsteady film on the plate so that the first peak is mainly dominated by the secondary atomization of the approaching droplets without wall contact. These arguments are consistent with the disappearance of the second peak away from the wall, as exemplified by figure 9(*b*), indicating that the large droplets generated by the film tend to stay close to the wall with relatively small vertical velocities, as discussed in §3.2. At the earlier time, t = 2 ms, the second peak at large size bands was less distinct, suggesting that, when the sizes of inflowing droplets decreased with the increasing velocities, splashes produced smaller size droplets which were not clearly discriminated in the size distribution from those of the inflowing droplets as in the later stages of injection. It is also true that smaller inflowing droplets

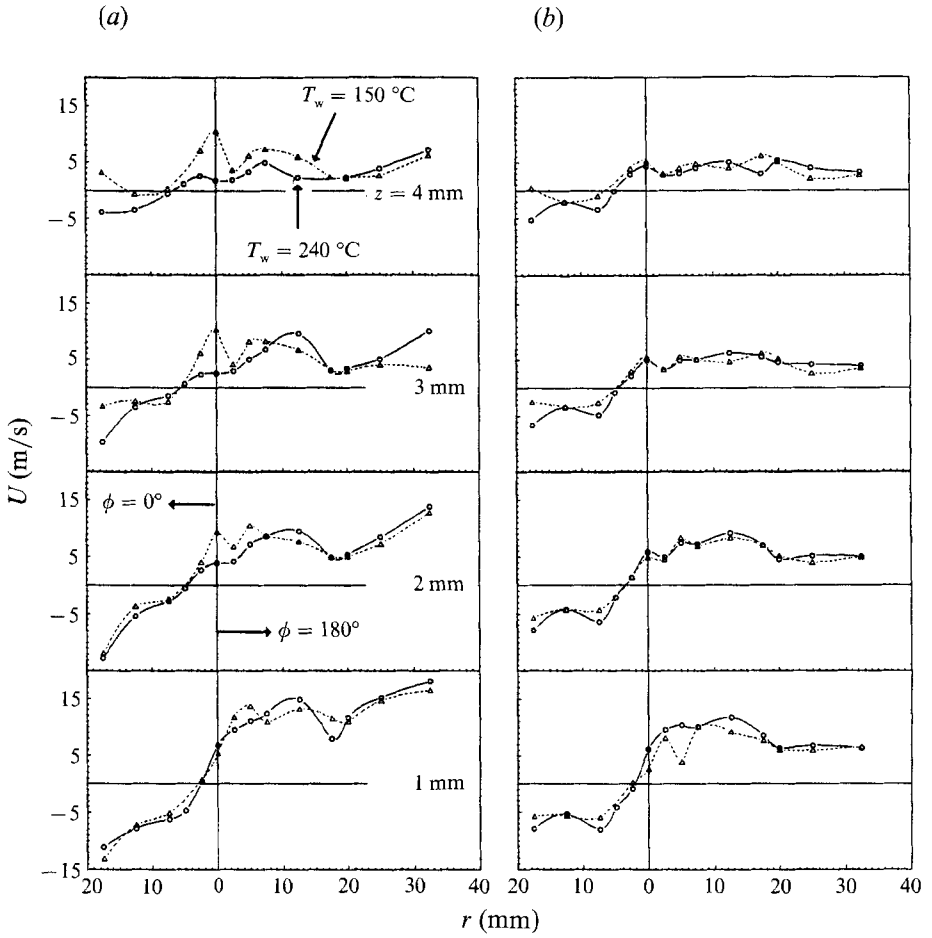

FIGURE 10. Variation of the mean radial velocity along the line of incidence; f_{inj} = 16.7 Hz with volume flow rate of 7.2 mm³/inj (*a*) t = 2 ms after needle lift; (*b*) t = 3.5 ms after needle lift.

could follow (Naber & Reitz 1988) the continuous phase within the impingement region better so that the impact of the droplets on the unsteady film occurred with more of a grazing incidence, resulting in less penetration into the film (Jayaratne & Mason 1964).

As one would expect from the distillation data in relation to the present wall temperature range, the results of drop size measurements so far and the observations of Özdemir & Whitelaw (1992*a*) reveal no evidence of a nucleate boiling or vapour bubbles but a spatially continuous and temporally unsteady film deposited on the plate. Impingement on the film is different from that on dry surfaces so that the film in this case prevents the formation of a vapour layer trapped between the impinging droplets and the wall and, therefore, prevails the spheroidal state for the droplet/hot-wall interaction.

The variations of droplet radial velocity along the line of incidence (figure 10) are similar in the vicinity of the impingement region for the two surface temperatures and injection phases to that the magnitude of the radial velocity increases from zero at the virtual origin to a maximum followed by a decrease to a constant level, except that it tends to further increase at large radial distances for t = 2 ms as in figure 10(*a*). In the vicinity of impingement, the trend of the droplet radial velocity resembles that of the

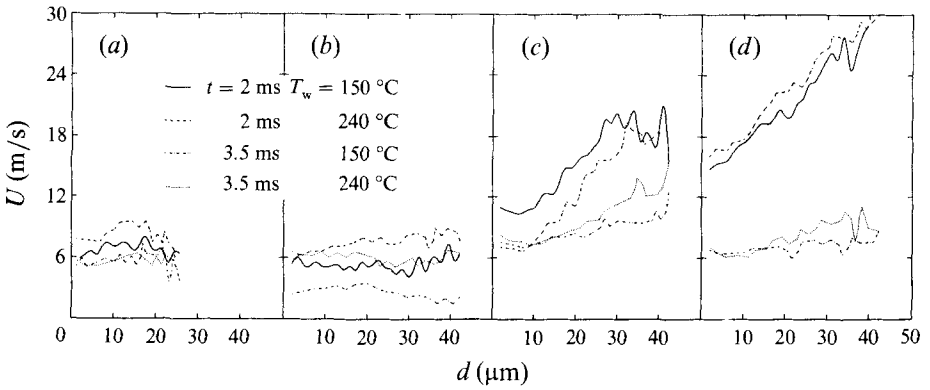

FIGURE 11. Velocity-size correlations at $z = 1$ mm. (*a*) $r = 12.5$ mm along the $\phi = 0°$ direction; (*b*) $r = 0$, geometrical impingement point; (*c*) $r = 17.5$ mm along the $\phi = 180°$ direction; (*d*) $r = 32.5$ mm along the $\phi = 180°$ direction.

steady single phase jet impingement (Özdemir & Whitelaw 1992*b*), so that the virtual origin of the wall flow is located on the $\phi = 0°$ line at a distance from the geometrical impingement point which increases with wall distance and this is consistent with the obliqueness of the inflowing jet. The magnitude of the radial velocity decreases away from the wall. It has been argued (Rumscheidt & Mason 1961; Torza, Cox & Mason 1972; Clift, Grace & Weber 1978) that droplet breakup depends on the rate at which the strain is applied as well as the magnitude of the strain so that the higher rate of strain in the impingement region leads to tiny satellite droplets. Therefore, considering the mean flow field of steady single-phase jet impingement reported by Özdemir & Whitelaw (1992*b*) as representative of the continuous phase, the strain would be expected to be highest at the virtual origin of the wall flow around which the radial spreading occurs in opposite directions. Since the distance of the virtual origin to the geometrical impingement point shifts towards the $\phi = 0°$ direction with wall distance, owing to the angled impingement, the region of the fragmental breakup should follow a similar trend.

Apart from buoyancy forces, which may rearrange the mean pressure field and the velocity, the thermal condition at the plate would also be expected to change the size distribution and so the distribution of the velocity among different size classes. The first mechanism had negligible influence on the mean flow field as the inertial forces would be considerably higher than the buoyancy forces. However, it is of note that, despite the differences seen in the variation of droplet size along the line of incidence for two surface temperatures at $t = 2$ ms, similar variations of the radial velocity along the line of incidence for the same two temperatures indicate that the kinematics of the radial spreading do not depend on the size distribution of the droplet field and are determined mainly by the nozzle exit conditions as in the single-phase flows. This point is confirmed by figure 11, which shows no size–velocity correlation when the velocity is less than 10 m/s. However, at large radial distances along the $\phi = 180°$ direction (figure 11*c*, *d*), the mean radial velocity increases with diameter at the earlier stage of the injection, $t = 2$ ms, for both wall temperatures and this is consistent with the trend of increasing velocities. Notice that this is not the case at the later stage of injection, $t = 3.5$ ms, when the mean radial velocity was smaller.

The r.m.s. values of the radial velocity (figure 12) have a similar variation at both surface temperatures and, even though there is scatter, it is clear that they increase with radial distance at the earlier stage of injection $t = 2$ ms, consistent with the mean

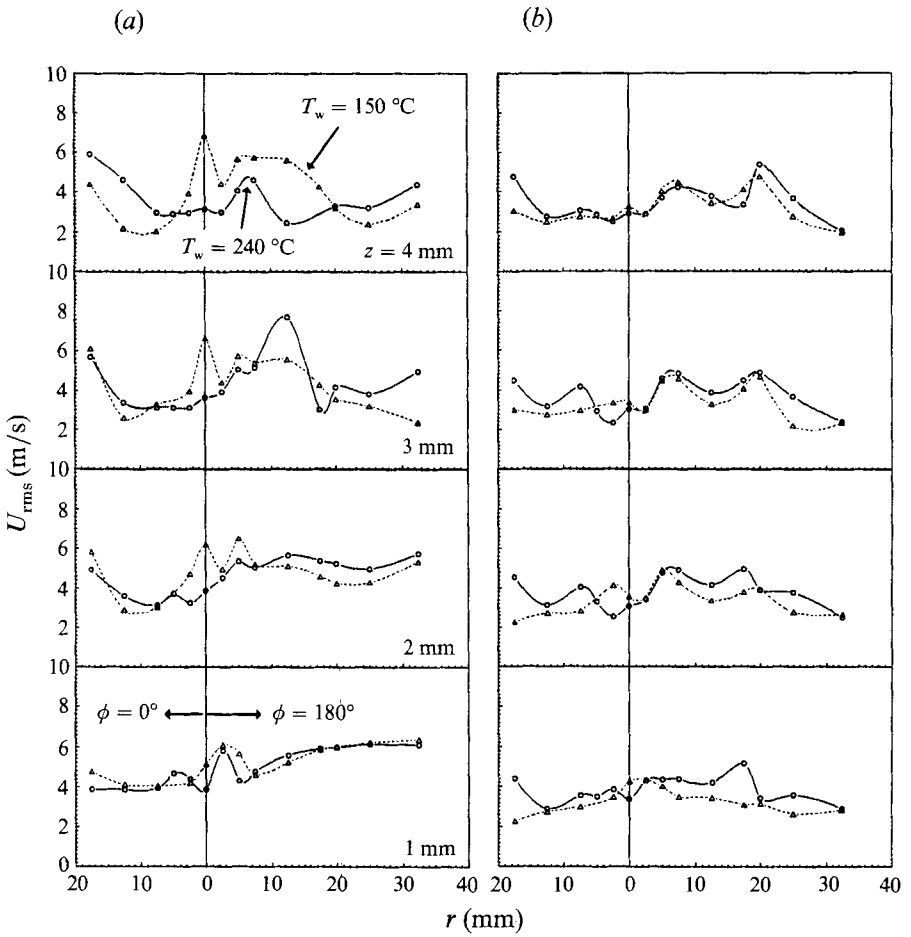

FIGURE 12. Variation of the r.m.s. of the radial velocity along the line of incidence; f_{inj} = 16.7 Hz with volume flow rate of 7.2 mm³/inj (*a*) t = 2 ms after needle lift; (*b*) t = 3.5 ms after needle lift.

velocities. Despite the decreasing mean velocities away from the wall, the r.m.s. values increase with distance from the wall, particularly for small radial distances along the $\phi = 180°$ direction since the flow at these positions corresponded to the free shear layer of the inflowing jet where turbulence intensity was relatively large. At t = 3.5 ms and at large radial distances, the r.m.s. decreases along the $\phi = 180°$ line whereas it increases along the $\phi = 0°$ line, particularly for T_w = 240 °C. It is interesting to note that there is no change in the r.m.s. velocity with wall distance at the later stage of injection, contrary to the earlier phase of injection. It should be recognized that the r.m.s. values were obtained over all droplet size classes and include the effects of the velocity variations of each droplet size class as well as the variations of the mean velocity with the droplet size. However, since there was no correlation between the droplet size and mean radial velocity, the r.m.s. represents the effects of velocity variations.

It is known (Middleman 1974) that, the droplets in a turbulent field can be subjected to the disruptive energy of the turbulent fluctuations associated with eddies of lengthscales smaller than the droplet diameter but, since the largest average droplet diameter was around 100 μm and smaller than the smallest dissipative eddy size associated with the continuous phase (Özdemir & Whitelaw 1992*b*), the effect of the

fine scale turbulence on the breakup of droplets within the impingement region should be less than that due to the mean flow strain so that the turbulence would not contribute much to the breakup mechanism without direct wall contact. On the other hand, the large-scale coherent motion of the steady wall jet described by Özdemir & Whitelaw (1992*b*) could contribute to the large-scale transport of the droplets to increase the correlation between the variation of the film thickness and the size characteristics of the wall jet. It can be conjectured that the oscillatory motion of the suspended droplet field, which is shown in §3.2 to play a key role in the mass transport from the film, corresponds to the coherent motion for the discrete phase of the unsteady two-phase jet impingement. As shown by the stability analysis of Özdemir (1991), the mean flow field can generate large-scale deterministic motion but the conditions for existence of the large structures in a time-dependent mean flow remain uncertain, together with their relationship to the timescale of the mean flow.

3.2. *Interfacial activity of the droplet field*

The characteristics of the interfacial activity were inferred from the space–time variation of the vertical droplet velocity measured with the laser-Doppler velocimeter in the immediate vicinity of the wall. The ensemble-averaged time histories for the two wall temperatures (figure 13) reveal an apparent wave structure which is coherent in phase with amplitude varying along the line of incidence. This recalls the mechanism of wave generation when a secondary flow exists parallel to a liquid surface at relatively high velocities, leading to atomization due to the material torn from the interface. In these cases, the rupture of the thin film has been known to take place because of the growth of the ripples at the air–film interface, which stem from Kelvin–Helmholtz instability (Woodmansee & Hanratty 1969; Hanratty 1983). However, some features of the wave structure contradict this concept. First, the propagation direction of the Kelvin–Helmholtz waves generated by the radial flow should be radially outwards so that the resulting transverse structure could be coherent in phase along the closed curves such as the egg-shapes seen in figure 4 of Özdemir & Whitelaw (1992*b*). The transverse structure of the wave in figure 13 is coherent in phase along the line of incidence as if a plane wave so that the propagation direction of the wave can only be perpendicular to the line of incidence, and it was concluded that the phenomenon was not related to interfacial waves. It can, however, be explained by the pulsatory impingement of the spray onto the film surface which introduces vertical oscillations in the droplet field in the vicinity of the interface by triggering a chain of ejection-and-reimpact of droplets during the period between the spray arrivals at a rate faster than the injection frequency so that the resulting phenomenon is perceived as a wave structure. In other words, a droplet cloud exists between injections and is radially (nearly) stagnant but moves as a whole up and down over the film so that the number of droplets in the cloud decreases with time while the individual droplets become smaller, partly owing to mass transferred to the film during coalescence with the film. This vertically oscillating droplet cluster in the vicinity of the film was swept radially outwards by the wall jet flow caused by the arrival of the next injection. This argument is supported by the fact that the amplitude of the transverse wave structure showed greater variation in the earlier stages of injection since agitation by the spray is not uniform over the film surface but rather in the form of discrete penetrations.

Although the analysis of deformations of the film interface by the pulsatory impingement of droplets and the subsequently induced vertical oscillations of the droplet field over the film is more complicated than the impact and rebounce of a single droplet, as for example Jayaratne & Mason (1964), the mechanisms seem to be similar.

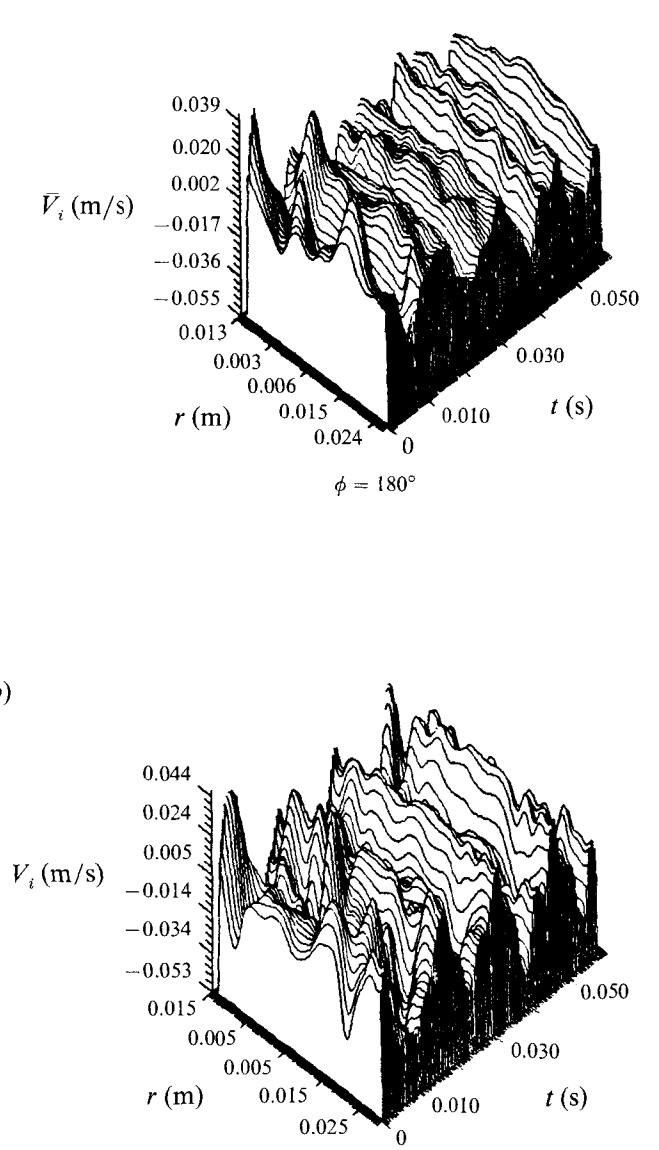

FIGURE 13. Wave structure of the interfacial activity with period; (*a*) T_r = 17.5 ms at a wall temperature T_w = 240 °C; (*b*) T_r = 14.5 ms at a wall temperature T_w = 150 °C; f_{inj} = 16.7 Hz with volume flow rate of 7.2 mm³/inj.

Thus, it is known from the impact of single droplets that a large proportion of the kinetic energy of the inflowing droplets is absorbed by the interface during penetration to generate the interfacial waves so that the ejected droplets have smaller vertical velocities and stay close to the interface. This argument is in agreement with the results of figure 9(*b*) so that the second peak of the size distributions due to the ejected droplets disappeared away from the wall. Also, when this mechanism of bursts of droplets from the interface exists, the frequency of the oscillations of droplets near the interface is expected to decrease with increase in wall temperature, as the surface tension decreases.

Consistent with the above argument, the periodic time of the wave motion in figure 13 increased from 14.5 ms for T_w = 150 °C to 17.5 ms for 240 °C, although the

mechanism of droplet ejection can be influenced the variations of film thickness (Türkdoğan 1966) and the effects of the temperature difference between the heated film on the surface and incoming droplets. In the latter case, the penetration of low-temperature droplets into warmer thin film is known to produce local changes in the temperature of the film leading to thermally-induced fluctuations of interfacial tension so that Marangoni-type instabilities (Austin, Ying & Sawistowski 1966; Skiepko & Panas 1989) can be significant at the interface introducing interfacial turbulence (Ellis & Biddulph 1966).

Another influencing factor to be mentioned on the mechanism of the ejection-and-reimpact of droplets is the gravitational force which determines the amplitude of the vertical oscillations of the suspended droplet field. However, it should be emphasized that since the plate was placed horizontally, the gravitational force had no preferred direction of influence for the radial transport of droplets which depends on the azimuthal distribution of the momentum of the two-phase wall-jet formed after impingement. Measurements of the wall pressure and temperature in an impinging jet (Özdemir & Whitelaw 1992*b*) show that the azimuthal distribution of the radial momentum and passive scalar in the vicinity of the wall is determined by the angle of impingement. Therefore, it can be concluded that when the plate in placed horizontally and approaching velocities are high, the angle of impingement is more important than the gravitational force for the factors which determine the distribution of the steady film thickness.

3.3. *Correlation between the droplet size of the two-phase wall jet and the dynamics of unsteady film thickness*

As explained in the introduction, the impingement of unsteady sprays on heated surfaces can also lead to an unsteady film which can be envisaged as the combination of a steady and a time-dependent component. The behaviour of the film depends on the velocity and size characteristics of the liquid phase of the incoming jet and on the thermal environment in the vicinity of the wall. Understanding of the dynamics of the unsteady film can provide information on evaporation and on the kinematics of mixing. Also, it has been shown that the penetration of droplets into the film results in the release of droplets of a different size-class to the wall jet and the mechanisms of further breakup and coalescence are correlated with the space–time structure of the film. The spray and two-phase flow after impingement were characterized by the laser diffraction and phase-Doppler techniques of the previous sections, but a proportion of the spray fluid is deposited in the form of a liquid film so that the mass balance demands knowledge of film thickness as a function of wall coordinates and time. The results of the new measurement technique (Özdemir 1991; Özdemir & Whitelaw 1992*a*) providing detailed information of the dynamics of unsteady films are, thus, considered in the light of present measurements.

The above description of the interaction between the wall jet droplet field and the unsteady film allows a semi-empirical relation for the droplet transport by the wall jet. As shown by Özdemir & Whitelaw (1992*a*), the contribution of evaporation to the dynamics of the unsteady film was negligible within the timescale of one injection cycle compared with the direct mass transfer by the ejected droplets so that the film thickness can be assumed to vary with the local values of the radial velocity and characteristic droplet size of the wall jet flow above it, i.e.

$$h_t = g(U, d_{32}, \mu, \sigma), \tag{3}$$

where h_t is the total film thickness and g refers an arbitrary functional relationship.

Note that, since the interfacial tension and viscosity play an important role in the dynamics of droplet ejection (Jayaratne & Mason 1964), the material properties such as dynamic viscosity, μ, and surface tension, σ, are also included. Equation (3) can also be expressed as

$$h_t = \alpha_1 (U)^{\alpha_2} (d_{32})^{\alpha_3} (\mu)^{\alpha_4} (\sigma)^{\alpha_5}. \tag{4}$$

For a physically consistent equation, the dimensional homogeneity implies that $\alpha_2 = \alpha_4$, $\alpha_3 = 1$, and $\alpha_5 = -\alpha_4$ or

$$\frac{h_t}{d_{32}} = \alpha_1 \left(\frac{U\mu}{\sigma}\right)^{\alpha_2}, \tag{5}$$

which can be put in the form

$$\frac{h_t}{d_{32}} = \alpha_1 \left(\frac{We}{Re}\right)^{\alpha_2}, \tag{6}$$

where $We = \rho U^2 d_{32}/\sigma$ and $Re = U d_{32}/\nu$.

Bearing in mind that a large proportion of the thickness variation was due to the droplets ejected from the film, rather than to evaporation, the mass balance gives

$$h = \alpha_6 d_{32},$$

where α_6 is a constant, so that, with the use of (6), one can obtain

$$\frac{h}{h_t} = \alpha_7 \left(\frac{Re}{We}\right)^{\alpha_2}. \tag{7}$$

Substituting $h_t = h + h_s$ (where h and h_s are unsteady and steady components of the film thickness, respectively) into (7) yields

$$\frac{h}{h_s} = \frac{1}{\alpha_8 \left(\frac{We}{Re}\right)^{\alpha_2} - 1}. \tag{8}$$

Equation (8) will be referred to as the droplet transport equation for the wall jet and expresses the coupling between the dynamics of the film thickness and the droplet field of the wall jet in terms of the local dimensionless parameters, h/h_s, We and Re. Equation (8) can be further refined by considering that We was at least two orders of magnitude larger than Re so that

$$\alpha_8 \left(\frac{We}{Re}\right)^{\alpha_2} \gg 1, \tag{9}$$

and, thus,

$$\frac{h}{h_s} = \alpha_9 \left(\frac{Re}{We}\right)^{\alpha_2}, \quad \text{where } \alpha_9 = \frac{1}{\alpha_8}. \tag{10}$$

The last form of the droplet transport equation requires knowledge of the steady film thickness, h_s, as well as We and Re. Since h_s was not measured by Özdemir & Whitelaw (1992*a*), the constants α_2 and α_9 remain undetermined and, thus, additional experimental study is required for finalizing the droplet transport equation.

4. Conclusions

4.1. *Mechanisms of atomization and effects of the approaching conditions of the inflowing droplet field and the temperature of the wall*

Two mechanisms of secondary atomization have been identified for the impingement of a two-phase jet on a heated plate. The first was due to the strain acting on the droplets by the continuous phase of the flow within the impingement region and was

promoted by the thermal effects penetrated from the wall. This mechanism is referred to as the secondary atomization without direct wall contact and resulted in fragmental breakup of large droplets into tiny droplets which dominated the average droplet size away from the wall. The approaching velocity of the inflowing droplets to the plate was particularly important for this type of breakup so that higher velocities resulted in increased rate of strain within the impingement region and, consequently, the wall temperature promoting secondary atomization shifted towards lower values. Since the strain was lower at large radial distances, this mechanism was mainly effective within the impingement region. The second mechanism, referred to as secondary atomization with direct wall contact, was the atomization of the film deposited on the wall with the impingement of the inflowing two-phase jet. With the penetration of high-speed inflowing droplets into the film, liquid mass was raised up into the two-phase medium owing to splashes from the film so that a new size class with larger droplets was generated with the addition of mass to the penetrating droplets directly from the film. The resulting large droplets tended to stay close to the wall within the impingement region with small vertical velocities and were perceived as a second peak at large size bands of the droplet size distribution in the immediate vicinity of the wall and shifted the average droplet size towards larger values. The secondary atomization with direct wall contact also caused strong correlation between the variation of the unsteady film and the droplet size of the two-phase wall jet so that, at some stage of injection ($t = 2$ ms), both exhibited three peaks at the same radial locations along the line of incidence. It can be concluded that the correlation initiated with the splashes from the film with the arrival of the inflowing droplets and continued with the oscillatory interfacial activities of the droplet cloud above the film.

4.2. *Evolution of the correlation between unsteady film thickness and the size characteristics of the wall jet droplet field*

The space–time structure of the film reported by Özdemir & Whitelaw (1992*a*) showed similar features for two wall temperatures so that the increase in evaporation rate with the wall temperature and its contribution to the dynamics of the unsteady film were marginal compared to the mass transport by ejected droplets. In between the injections, the suspended droplet field above the film oscillated normal to the plate as a cloud so that the impact of large droplets on the film resulted in coalescence with the film and the ejection of smaller numbers of small droplets. This settling process also explains the persistence of the intermediate peak in the distribution of unsteady film thickness till the end of the injection cycle as reported by Özdemir & Whitelaw (1992*a*). However, the unsteady wall jet flow caused by the arrival of the spray at the plate swept the vertically oscillating droplet cloud radially outwards so that the resulting radial transport enhanced the correlation between the dynamics of the unsteady film and the size characteristics of the unsteady wall jet. It should be emphasized again that the key mechanism for the correlation was the coupling introduced by a series of events which was initiated with the atomization by direct wall contact and continued with the subsequent oscillatory motion of the droplet field. Based on this phenomenological description, a correlation between the thickness variation and the local parameters such as Weber number, We, and Reynolds number, Re, was found and expected to hold at large radial distances where the mean radial velocity was the only velocity scale for transport.

The authors are grateful to the Ford Motor Co. UK Ltd and to the European Commission (Contract number JOULE-0056-C(MB)) for financial support.

REFERENCES

ASHGRIZ, N. & POO, J. Y. 1990 Coalescence and separation in binary collisions of liquid drops. *J. Fluid Mech.* **221**, 183–204.

AUSTIN, L. J., YING, W. E. & SAWISTOWSKI, H. 1966 Interfacial phenomena in binary liquid–liquid systems. *Chem. Engng Sci.* **21**, 1109–1110.

BRACCO, F. V. 1985 Modelling of engine sprays. *SAE Paper* 850394.

CLIFT, R., GRACE, J. R. & WEBER, M. E. 1978 *Bubbles, Drops and Particles*, pp. 339–347. Academic.

COSSALI, E. & HARDALUPAS, Y. 1992 Comparison between laser diffraction and phase-Doppler velocimeter techniques in high turbidity, small width sprays. *Exps Fluids* **13**, 414–422.

CUMO, M. & FARELLO, G. E. 1967 Heated wall-droplet interaction for two-phase flow heat transfer in liquid deficient region. *Proc. Symp. on Two Phase Flow Dynamics, Eindhoven*, vol. 2, 1325–1357.

DIMITROV, D. S. & IVANOV, I. B. 1978 Hydrodynamics of thin liquid films. On the rate of thinning of microscopic films with deformable interfaces. *J. Colloid Interface Sci.* **64**, 97–106.

DODGE, L. G. 1984 Change of calibration of diffraction-based particle sizers in dense sprays. *Opt. Engng* **23**, 626–630.

ELLIS, S. R. M. & BIDDULPH, M. 1966 Interfacial turbulence measurements. *Chem. Engng Sci.* **21**, 1107–1109.

FELTON, P. G., HAMIDI, A. A. & AIGAL, A. K. 1985 Measurement of drop size distributions in dense sprays by laser diffraction. *Proc. 3rd Intl Conf. on Liquid Atomisation and Spray Systems, Imperial College, London*, ICLASS-85, IVA/4/1.

FUJIMOTO, H., SUGIHARA, H., TANABE, H. & SATO, G. T. 1983 Investigation on combustion in medium-speed marine diesel engines using model chambers. *Proc. of 15th Intl Congress on Combustion Engines, Paris*, CIMAC, D13.3.

GALLILY, I. & LA MER, V. K. 1958 On the behavior of liquid droplets after impinging on solid surfaces. *J. Phys. Chem.* **62**, 1295–1299.

HAMMOND, D. C. 1981 Deconvolution technique for line-of-sight optical scattering measurements in axisymmetric sprays. *Appl. Optics* **20**, 493–499.

HANRATTY, T. J. 1983 Interfacial instabilities caused by air flow over a thin liquid layer. In *Waves on Fluid Interfaces* (ed. R. E. Meyer), pp. 221–259. Academic.

HIRLEMAN, E. D., OECHSLE, V. & CHIGIER, N. A. 1984 Response characteristics of laser diffraction particle analyzer: optical sample volume extent and lens effects. *Opt. Engng* **23**, 610–619.

HOOGENDOORN, C. J. & HOND, R. DEN 1974 Leidenfrost temperature and heat-transfer coefficients for water sprays impinging on a hot surface. *Proc. Fifth Intl Heat Transfer Conference*, vol. 4, pp. 135–138.

HORI, M. & SUGIYAMA, H. 1980 Combined measurement by photography and gas sampling for combustion analysis in a diesel engine cylinder. *SAE Paper* 800986.

JAYARATNE, O. W. & MASON, B. J. 1964 The coalescence and bouncing of water drops at an air/water interface. *Proc. R. Soc. Lond.* A **280**, 545–565.

KATSURA, N., SAITO, M., SENDA, J. & FUJIMOTO, H. 1989 Characteristics of a diesel spray impinging on a flat wall. *SAE Paper* 890264.

LEFEBVRE, A. H. 1989 *Atomisation and Sprays*. Hemisphere.

MEYER, P. & CHIGIER, N. 1986 Dropsize measurements using a Malvern 2200 particle sizer. *Atomis. Spray Technol.* **2**, 261–298.

MIDDLEMAN, S. 1974 Drop size distributions produced by turbulent pipe flow of immiscible fluids through a static mixer. *Ind. Engng Chem., Process Des. Dev.* **13**, 78–83.

NABER, J. D. & REITZ, R. D. 1988 Modelling engine spray/wall interaction. *SAE Paper* 880107.

ÖZDEMİR, İ. B. 1991 Impingement of single and two-phase jets on unheated and heated flat plates. PhD thesis, Imperial College, University of London.

ÖZDEMİR, İ. B. & WHITELAW, J. H. 1992*a* An optical method for the measurement of unsteady film thickness. *Exps Fluids* **13**, 321–331.

ÖZDEMİR, İ. B. & WHITELAW, J. H. 1992*b* Impingement of an axisymmetric jet on unheated and heated flat plates. *J. Fluid Mech.* **240**, 503–532.

PANDIT, A. B. & DAVIDSON, J. F. 1990 Hydrodynamics of the rapture of thin liquid films. *J. Fluid Mech.* **212**, 11–24.

PEDERSEN, C. O. 1970 An experimental study of the dynamic behavior and heat transfer characteristics of water droplets impinging upon a heated surface. *Intl J. Heat Mass Transfer* **13**, 369–381.

RANZ, W. E. & HOFELT, C. 1957 Determining drop size distribution of a nozzle spray. *Ind. Engng Chem.* **49**, 288–293.

REITZ, R. D. & BRACCO, F. V. 1979 Ultra-high-speed filming of atomizing jets. *Phys. Fluids* **22**, 1054–1064.

REITZ, R. D. & BRACCO, F. V. 1982 Mechanism of atomization of a liquid jet. *Phys. Fluids* **25**, 1730–1742.

RUMSCHEIDT, F. D. & MASON, S. G. 1961 Particle motions in sheared suspensions; deformation and burst of fluid drops in shear and hyperbolic flow. *J. Colloid Interface Sci.* **16**, 238–261.

SKIEPKO, J. & PANAS, J. 1989 Instability of the motion of a spherical drop in a vertical temperature gradient. *Arch. Mech.* **41**, 811–820.

TORZA, S., COX, R. G. & MASON, S. G. 1972 Particle motions in sheared suspensions; transient and steady deformation and burst of liquid drops. *J. Colloid Interface Sci.* **38**, 395–411.

TÜRKDOĞAN, E. T. 1966 Fluid dynamics of gas jets impinging on surface of liquids. *Chem. Engng Sci.* **21**, 1133–1144.

WACHTERS, L. H. J., BONNE, H. & VAN NOUHUIS, H. J. 1966*a* The heat transfer from a hot horizontal plate to sessile water drops in the spheroidal state. *Chem. Engng Sci.* **21**, 923–936.

WACHTERS, L. H. J., SMULDERS, L., VERMEULEN, J. R. & KLEIWEG, H. C. 1966*b* The heat transfer from a hot wall to impinging mist droplets in the spheroidal state. *Chem. Engng Sci.* **21**, 1231–1238.

WACHTERS, L. H. J. & WESTERLING, N. A. J. 1966 The heat transfer from a hot wall to impinging water drops in the spheroidal state. *Chem. Engng Sci.* **21**, 1047–1056.

WOODMANSEE, D. E. & HANRATTY, T. J. 1969 Mechanism for the removal of droplets from a liquid surface by a parallel air flow. *Chem. Engng Sci.* **24**, 299–307.

YAO, S. C. & CAI, K. Y. 1985 Dynamics and heat transfer of drops impacting on a hot surface at small angles. *Proc. 3rd Intl Conf. on Liquid Atomisation and Spray Systems, Imperial College, London*, ICLASS-85. VII/B/1-11.

ZHANG, S. & GOGOS, G. 1991 Film evaporation of a spherical droplet over a hot surface: fluid mechanics and heat/mass transfer analysis. *J. Fluid Mech.* **222**, 543–563.